A Hierarchical Particle–Shell Architecture for Long-Term Cycle Stability of Li_2S Cathodes

*Feixiang Wu, Jung Tae Lee, Feifei Fan, Naoki Nitta, Hyea Kim, Ting Zhu, and Gleb Yushin**

The ever-increasing energy storage demands of laptops, mobile phones, cameras, electric tools, unmanned aerial vehicles, and cars have motivated research on safer, lighter, and lower cost rechargeable batteries. Commercial Li-ion batteries utilizing intercalation-type Co- and Ni- containing cathode materials suffer from natural toxicity, relatively high cost, and limited specific capacities. Conversion-type cathode materials may offer reduced cost and higher specific energy, particularly in combination with Li metal or Li alloy anodes.[1] Since 2009, the lithium–sulfur (Li–S) chemistry with the high theoretical energy of 2600 W h kg^{-1} has attracted great attention in the battery community.[2–5] Sulfur is abundant in the earth crust, cheap, and environmentally friendly. Each sulfur atom can bond to two lithium atoms forming lithium sulfide (Li_2S) and giving the theoretical capacity of 1675 mA h g^{-1}.

However, elemental S-based electrodes suffer from multiple limitations. For example, the low melting point of S (115 °C) readily induces evaporation of the active material under normal electrode drying conditions. Large expansion (≈79 vol%) of S during its lithiation to Li_2S may induce mechanical damages within electrodes or S-comprising composite electrode particles (particularly, if insufficiently large pores within composite particles obstruct such expansion), while polysulfide dissolution during cycling induces active material loss and increases cell resistance.[6–9] The presence of excessively large pores in composite particles can lower the volumetric capacity. In order to reduce polysulfide dissolution, a variety of approaches, including the optimization of electrolyte composition,[10,11] the use of metal oxide additives,[3,14] coating separators,[15] various protective shells on individual particles,[7,9,16] and the encapsulation of sulfur in a carbon with hierarchical pore structure,[17] have been explored and showed great promise, but further improvements are still critically needed.

Dr. F. Wu, Dr. J. T. Lee, N. Nitta, Dr. H. Kim, Prof. T. Zhu, Prof. G. Yushin
School of Materials Science and Engineering
Georgia Institute of Technology
Atlanta, GA 30332, USA
E-mail: yushin@gatech.edu
F. Fan, Prof. T. Zhu
Woodruff School of Mechanical Engineering
Georgia Institute of Technology
Atlanta, GA 30332, USA
Dr. H. Kim
Sila Nanotechnologies, Inc.
Alameda, CA 94501, USA

DOI: 10.1002/adma.201502289

Compared with elemental S, the Li_2S cathode can pair with the anode materials, such as C, Si, and Sn, which do not contain Li, and thus the Li_2S cathode can offer improved safety. In addition, Li_2S does not further expand during cycling since Li is already incorporated into the structure, making it a strong candidate for S-based cathodes.[4,13,18–22] However, due to its high melting point (≈950 °C), it has been a challenge to encapsulate the nanosized Li_2S into hosts with porous and hierarchical structures. Even if the Li_2S/S particles are coated with protective shells, such protections are often insufficiently robust and fail during handling or cycling due to the repeated volume changes and resultant mechanical degradation.[7,19,21,23–25] When only a small portion of the particles fails, the dissolved polysulfides still form insulating layers on the surface of both electrodes, increase electrolyte viscosity, and lead to cell failure.[19] Furthermore, the low electrical conductivity of both S and Li_2S requires the use of small nanoparticles for minimizing polarization during cycling. This could also be undesirable as small nanoparticles exhibit higher specific surface areas and thus faster dissolution.

Here we construct a hierarchical nanocomposite particle–shell architecture of Li_2S cathode, which offers a multilevel protection against damages within protective coatings of particles. This architecture not only drastically reduces internal stresses within outer shells, but also allows one to achieve high-capacity utilization of insulative Li_2S for a relatively large size of the composite particles. The proposed particle architecture and general synthesis route could be effectively utilized for building electrochemical cells with a variety of other conversion-type cathode materials, which undergo significant volume changes during cycling and suffer from undesirable interactions with electrolytes and low conductivity.

Figure 1 illustrates the overall concept for the nanocomposite particle–shell architecture aimed to enhance the mechanical stability of electrodes containing the volume-changing active materials, such as Li_2S. In the case of simple core-shell particles (Figure 1a), failure of the shell may lead to catastrophic consequences for the electrode, once Li_2S has a direct contact with electrolytes. Overbuilding the shell thickness would increase the volume of inactive shell materials and may increase Li^+ transport resistance. However, when multiple particles are first embedded into the protective composite matrix and then additionally protected by an outer protective shell so as to achieve a first level of hierarchy, the failure probability would be greatly reduced (Figure 1b). Indeed, fractures within the outer shell would be mitigated by the presence of the protective material matrix. After achieving the second level of hierarchy in the particle design (Figure 1c), fractured materials within both the

ADVANCED MATERIALS
www.advmat.de

www.MaterialsViews.com

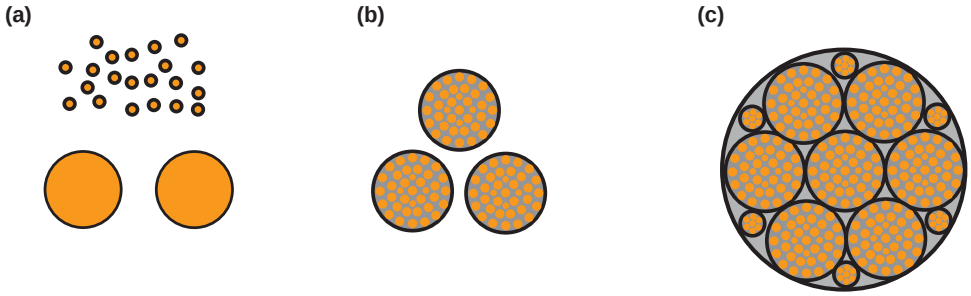

Figure 1. A concept of hierarchical particles' shelling for enhanced mechanical stability of volume-changing active materials, such as Li_2S. Particles exhibiting three levels of enclosing hierarchy are shown: a) zero (small and medium size particles), b) one, and c) two. Failure of a shell in a primary particle in (b) could be mitigated by a second-level shell. Failure of both a primary shell and a second-level shell in (c) could be mitigated by a shell at the third level.

zero and first level of hierarchy would be further protected by the outermost shell.

Importantly, the hierarchical particle–shell architecture can significantly reduce stresses within the shells. **Figure 2** shows results of our numerical simulations (see details of the model in the Supporting Information), where the outer shell is assumed to be made of carbon that does not change volume during extraction of Li from Li_2S. Particles exhibiting a zero-level hierarchy (Figure 2a) are assumed to have weaker spots at the interface between the Li_2S particle and the shell in order to accommodate the particle shrinkage (during Li extraction) via formation of wrinkles. As a result, large hoop tension induced in the crests of the wrinkles can induce local fracture of the coating, leading to a loss of polysulfides during subsequent cycles. In comparison, composite particles exhibiting the first level of hierarchy in our model (Figure 2b) have a number of small Li_2S particles embedded in the elastic porous carbon matrix and further coated with a carbon outer shell. In this case, the volume decrease in active particles occurring during delithiation will be effectively accommodated by the deformation of the porous carbon matrix having a low stiffness and high deformability. Now, even in the case when active Li_2S nanoparticles exhibit a perfect bonding with the porous carbon matrix and the core of the composite particles exhibit a perfect bonding with the

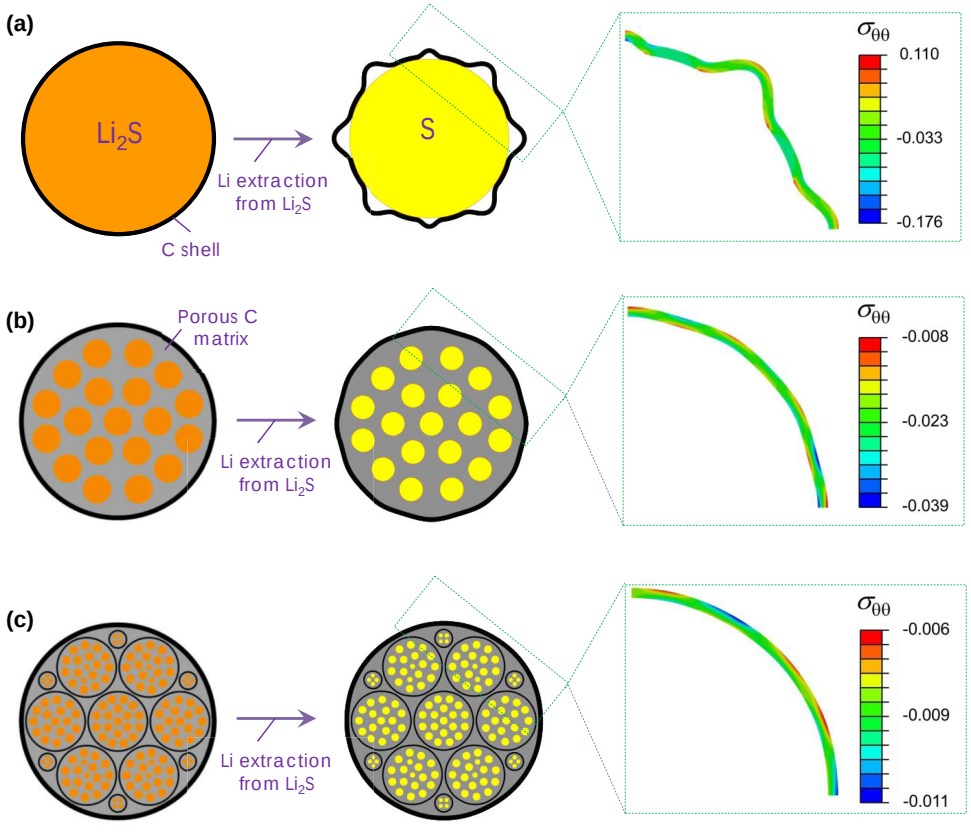

Figure 2. Results of the numerical modeling, showing significant reduction of the hoop stress (normalized by Young's modulus of carbon) within the outer shells of the Li_2S–C composite particles with the increasing level of the hierarchy in particles' shelling: a) zero level; b) first level; c) second level.

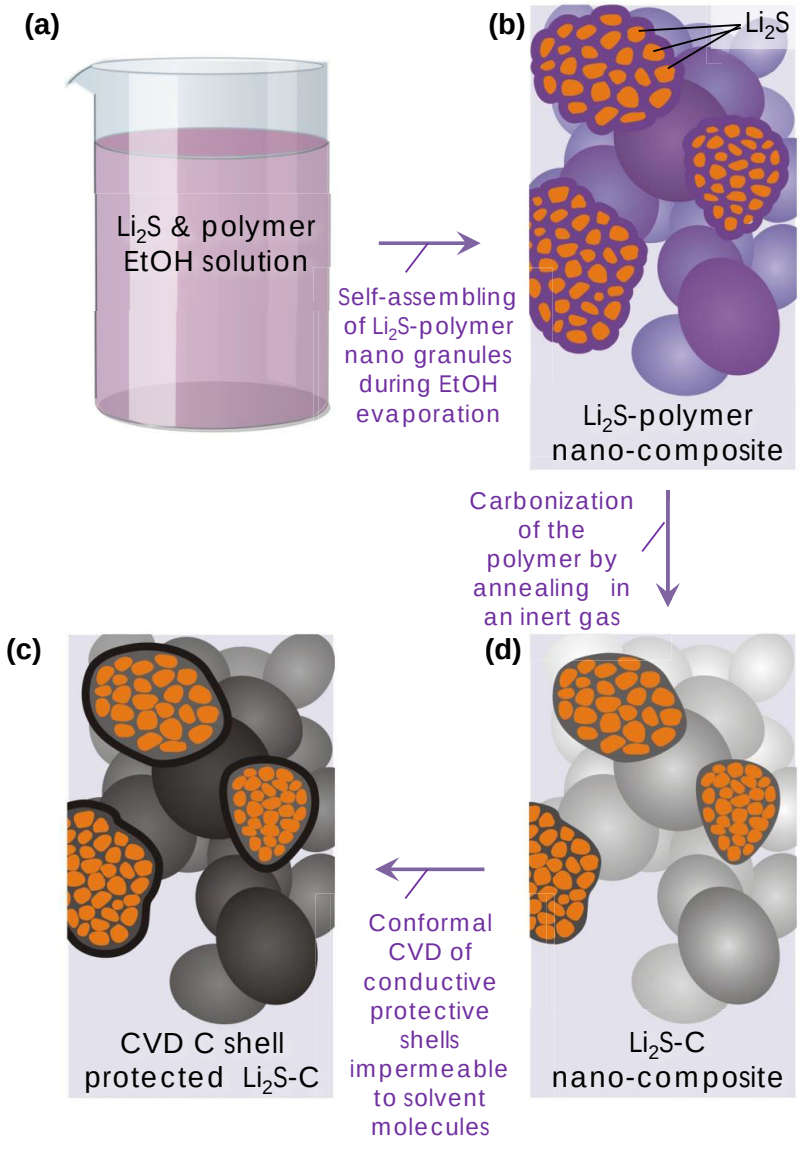

Figure 3. Schematic of the process flow for the scalable formation of hierarchical C–Li2S–C nanocomposite nanoparticles, involving both wet chemistry and vapor deposition approaches.

carbon outer shell, stresses induced in the shell are significantly lower (Figure 2b). Finally, particles exhibiting the second level of hierarchy in our model result in a further reduction of stresses within the outer carbon shell (Figure 2c).

While the advantages of the proposed particle–shell architecture are broadly applicable, here we demonstrate the clear improvements in the capacity, rate, and cycle stability of hierarchical Li_2S particle–C shell cathodes. We further limit our experimental results to particles having just one level of hierarchy. Similar to the description of our model system above (Figure 2b, c), we have selected elastic disordered porous carbon matrix and more rigid carbon outer shell as protective media that are electrically and ionically (Li^+) conductive for Li_2S. **Figure 3** shows schematics of the synthesis steps involved. First, both carbonizable polar polymer and Li_2S are dissolved in anhydrous ethanol (EtOH) (Figure 3a), following our previous work on the discovery of a high solubility of Li_2S in such an environmentally friendly solvent and the absence of Li_2S alcoholysis.[4,18] Second, evaporation of ethanol to a level exceeding the Li_2S solubility limit induces homogeneous nucleation of small Li_2S nanoparticles, which become coated with a polar polymer chain and self-assembled into larger Li_2S–polymer nanocomposite granules (Figure 3b). The produced nanocomposite powder is annealed at a temperature sufficiently high to induce polymer carbonization (such as 700 °C, in our case). As a result, the particles are transformed into C–Li_2S nanocomposites comprising smaller Li_2S nanoparticles uniformly distributed within a highly deformable, porous carbon matrix (Figure 3c). Such a process is enabled by the high melting point of Li_2S. The final step involves deposition of the hard carbon coating on the nanocomposite particle surface by atmospheric pressure chemical vapor deposition (CVD) (Figure 3d). While other approaches may also be used to achieve hierarchical particle–shell architecture and be sufficient for our proof-of-concept studies, we utilized this fabrication method due to our expertise in this field, as well as the simplicity and scalability of the proposed process.

Figure 4 and **5** show results of microstructural characterizations of the hierarchical particle–shell Li_2S–C nanocomposites produced according to the steps in Figure 3. The uniform and spheroidal Li_2S–C nanocomposite particles (step Figure 3c) range from 100 to 300 nm in size (Figure 4a). CVD deposition of C on the nanocomposite surface yields a smooth and uniform layer without noticeably changing particle size distribution and morphology (compare Figure 4a,b). Figure 4c shows results of energy dispersive X-ray spectroscopy (EDS), demonstrating the lack of elements other than S and C and ≈40 wt% fraction of C in Li_2S–C nanocomposite. We expect that further material optimization may reduce C fraction without sacrificing composite performance characteristics. Since some of the composite particles are visibly linked together, the actual level of hierarchy in our particles is somewhere between one and two (Figure 2).

Previous reports (see, e.g., ref.[19]) showed the presence of side reactions between pure Li_2S and acetylene and formation of undesirable phases during the C CVD at comparable conditions. In contrast, our X-ray diffraction (XRD) studies showed the presence of only pure and single crystalline phase of Li_2S before and after the C CVD step (Figure 4d). We propose that the high purity of the components and the presence of the carbon matrix surrounding nanosized Li_2S effectively prevent side reactions between the Li_2S and acetylene. X-ray

ADVANCED MATERIALS
www.advmat.de

www.MaterialsViews.com

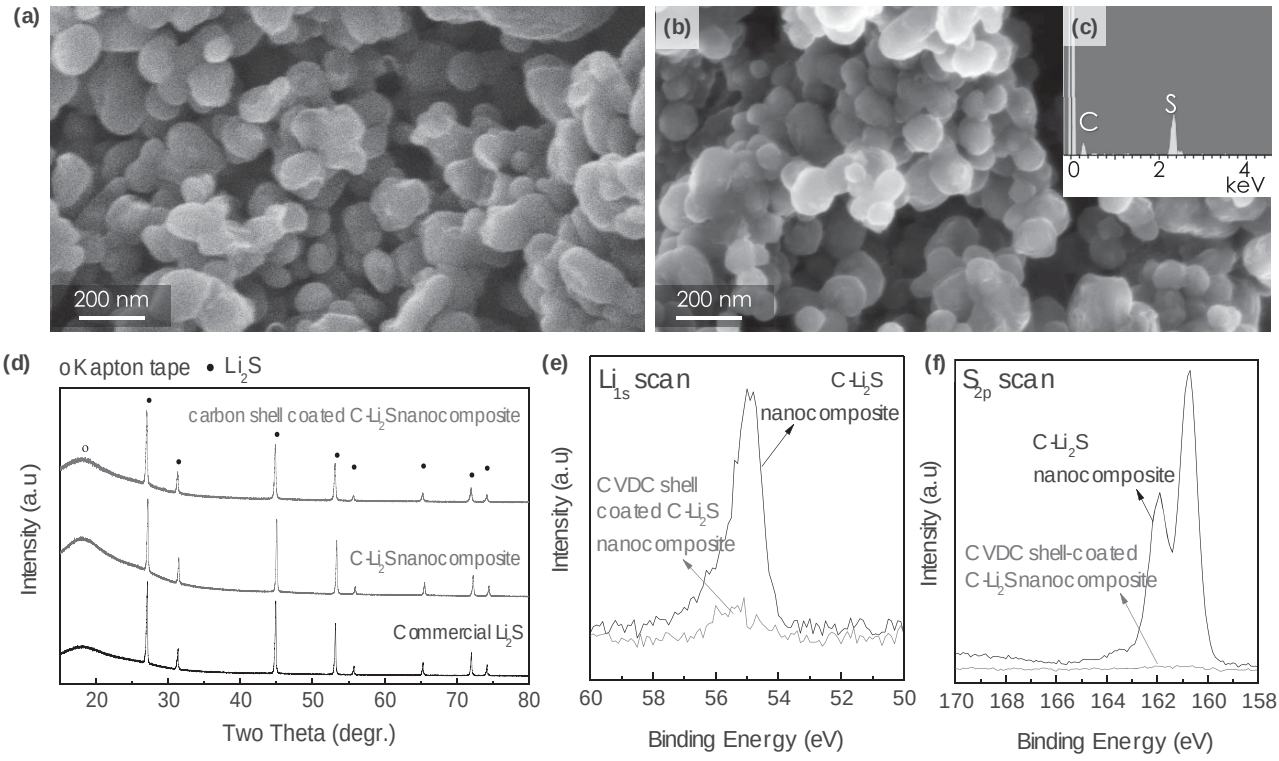

Figure 4. Structural and chemical characterization of the synthesized hierarchical nanocomposite samples before and after C shell deposition: a) SEM images before and b) after the CVD shell deposition; c) EDS spectra of the C-shell enclosed composite; d) XRD patterns of the commercial Li_2S powder and the produced composite samples, showing formation of pure Li_2S; high-resolution XPS spectra of e) Li_{1s} and f) S_{2p} lines before and after C shell deposition on the produced C–Li_2S composite nanopowder, showing high conformity of the deposited shells.

photoelectron spectroscopy (XPS) studies further confirmed the lack of impurities and the high conformity of the CVD coatings. As expected, the high-resolution Li_{1s} and S_{2p} scans on the sample surfaces showed near disappearance of Li_{1s} and S_{2p} peaks after the CVD coating step (Figures. 4 e,f).

Transmission electron microscopy (TEM) studies revealed the distribution of Li_2S and C within the hierarchical nanocomposites. **Figures** 5a,b show TEM and scanning transmission electron microscopy (STEM) images of ≈100 nm Li_2S–C nanocomposite particles uniformly coated by a ≈10 nm carbon layer, which is much thinner than the 33 nm C shell in the previous report[19] using pure Li_2S as core and C CVD. Such a layer is expected to block the XPS signal from Li_2S, as previously observed (Figure 4e,f). The traces of Li detected (Figure 4e) could be related to a small amount of Li inserted into carbon at a high equilibrium potential. The normalized intensities of the EDS line scan across a typical hierarchical nanocomposite particle, performed in the STEM operational mode of the microscope, further confirmed the composition of the shell and the core of the particles (Figure 5c). High resolution TEM imaging revealed the uniform distribution of the Li_2S particles ranging from 5 to 20 nm within the amorphous carbon matrix and the turbostratic microstructure of the graphitic shell (Figure 5d,e), which is consistent with the XRD, XPS, and EDS results (Figure 4d,f, Figure 5c).

Electrochemical performances of the produced hierarchical particle–shell Li_2S–C nanocomposite particles were studied with Li-foil anodes in coin cells. Considering the possible exposure of cells to elevated temperatures in electric vehicle applications, we have conducted tests not only at ≈20 °C (room temperature) but also at 35 °C and 45 °C. At all the temperatures tested, the nanocomposite-based electrodes show near-theoretical capacities (**Figure 6**), which suggests that the Li_2S nanoparticles within the nanocomposite (Figures 3d and 5d) are well interconnected both electrically and ionically.

Conducting rate tests at different temperatures allows one to distinguish ionic from electronic polarization because electron mobility is virtually independent on small temperature variations. Increasing cell temperature from 20 to 35 and 45 °C clearly improved rate performance (Figure 6a) and reduced voltage hysteresis (compare Figure 6b with 6c,d). At a moderate temperature of 45 °C, the cell showed reversible capacities of 1020–1310 mA h g_s^{-1} at very high (for this chemistry) C rates of 5C–1C, respectively, which are even higher than the previously reported graphene/CNT/S nanocomposites.[26] Such remarkable rate performance and small hysteresis are due not only to small sizes of Li_2S nanocrystals and high electrical conductivity of carbon matrix (Figure 5d), but also to prevention of polysulfide dissolution and the related lack of resistive layers build-up on the surface of both electrodes,[8,11] as will be further demonstrated.

The voltage discharge profiles (Figure 6b,d) recorded at slow rates of C/10 to C/5 show a short plateau at ≈2.35 V versus Li/Li^+ and a single long plateau at ≈2.2 V versus Li/Li^+, close

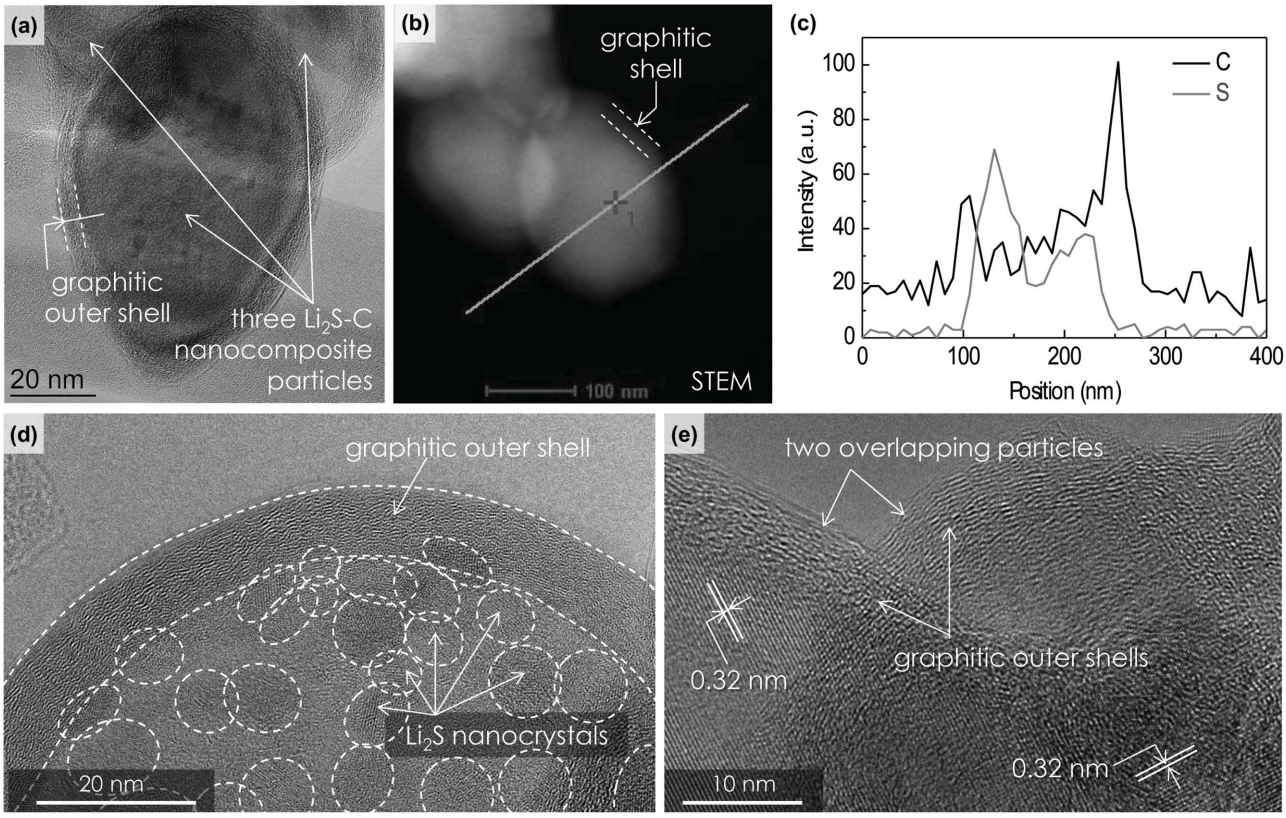

Figure 5. TEM characterization of the synthesized hierarchical nanocomposite samples: a) a low-resolution TEM image of the core–shell nanocomposite; b) an STEM image showing the projected sample density, c) normalized EDS line-scan profile, showing the presence of C shell along the line in (b), d) a high-resolution TEM image showing both the graphitic shell and Li_2S nanocrystals within amorphous carbon matrix, e) the highest resolution TEM image showing the inter-planar spacing within the nanocrystals coinciding with that of the (111) planes of Li_2S.

to the theoretical voltage. The first plateau corresponds to the formation of Li_2S_8.[5,27,28] Further lithiation is often believed to lead to the conversion between polysulfides soluble in electrolytes, such as Li_2S_6 and Li_2S_4 and eventual formation of insoluble Li_2S_2, consuming up to 50% of the total capacity.[5,27,28] The remaining 50% of the capacity, corresponding to the formation of Li_2S from Li_2S_2, is commonly observed to occur at a sloping region of the discharge curve, lowering the average voltage and the accessible cell energy density.[5,27] In our case, however, we observe a single and nearly flat plateau (particularly at elevated temperatures when Li^+ mobility is higher, see Figure 6d), which may suggest a direct conversion of Li_2S_8 to Li_2S. This difference from prior studies may be related to the lack of a direct contact between the active material and liquid electrolyte in our composite particles. We shall note, however, that Li_2S_8 is also a metastable phase that is commonly not seen in solid state Li/S batteries. Its formation during discharge may originate due to a particular interfacial chemistry in our Li_2S–C nanocomposites. We also cannot fully exclude a possibility that a very small amount of electrolyte species penetrated into the bulk of the composite particles through grain boundaries. However, as we will demonstrate, the Li_2S_8 built within the composite particles during initial discharge of the reduced S do not get lost to electrolyte even after extensive cycling.

Cycle stability studies at different rates and temperatures have been conducted on cells already exposed to rate tests (**Figure 7**a). A remarkable stability was demonstrated at all the temperatures, including 35 and 45 °C, when polysulfide dissolution (if allowed) would be significantly higher than at room temperature. Specific discharge capacities increase from ≈1000 to ≈1300 and to ≈1400 mA h g_s^{-1} with increasing temperature to 35 and 45 °C, respectively, at C/2 rate. Virtually no degradation could be detected within 100 cycles (Figure 7a), suggesting that polysulfide dissolution was successfully prevented using the hierarchical particle design.

Cycle stability of the hierarchical core–shell nanocomposite particles was studied at both room and elevated temperatures (Figure 7a). As expected, higher temperature or lower rates resulted in higher capacity utilization. All cells, however, showed excellent capacity retention with virtually no degradation within 100 cycles. In order to evaluate the ability of the hierarchical core–shell particle architecture to provide long-term resilience against defect formation during cycling, several cells were cycled for 300–600 cycles, demonstrating remarkable stability (Figure 7b). The majority of the previous studies on Li_2S could not achieve cycle stability in excess of 100 cycles.[23,29] A few recent studies on the Li_2S cathode employing a core–shell architecture (corresponding to the zero-level hierarchy) showed impressive 200–400 cycles.[19,20,25] However, their lower

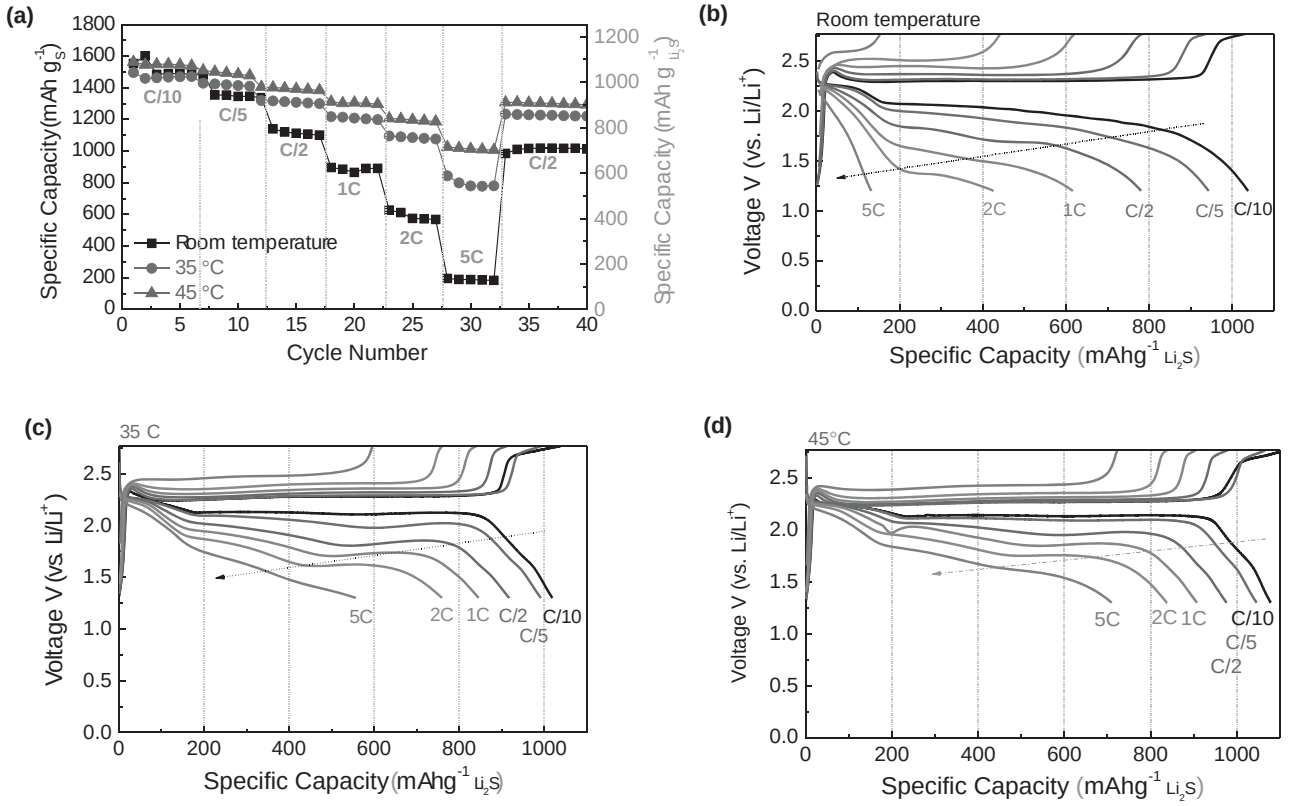

Figure 6. Electrochemical characterizations of the hierarchical C–Li2S composite nanopowder samples: a) discharge capacity at different C-rates and temperatures; b,c,d) charge–discharge profiles corresponding to different C-rates and recorded at: b) room temperature, c) 35 °C, and d) 45 °C.

capacity utilization and significantly more rapid fading suggest formation of sufficiently large defects and cracks in their shells, which lead to cell degradation and failure. The combination of high-capacity utilization, rate performance and cycle stability of the hierarchical particle–shell architecture of the C–Li_2S reported in this work is so far the best to our knowledge and likely can be further improved. Therefore, in spite of only small structural modifications we employed compared to prior art, we demonstrate significant improvements in both capacity and stability over previous studies, where either pure Li_2S was covered with a single shell[19,20,25] or when S was used in hierarchical porous composites.[17]

Postmortem studies of the electrodes were conducted after 100 and 200 cycles at 35 and 45 °C, respectively, in order to identify possible damages within particles (Figure S1, Supporting Information). The cycled electrodes showed only the presence of a smooth solid electrolyte interphase (SEI) layer and the lack of reprecipitation of any Li_2S, which are hard to be achieved in regular Li–S cells due to polysulfide dissolution that becomes particularly significant at elevated temperatures.[8,11,12] Similarly, we also could not detect any cracks on the particle surface (compare Figure S1a and S1b, Supporting Information). To further confirm the lack of polysulfide dissolution, we conducted EDS on the electrodes and within experimental error observed no change in the chemical composition of the electrodes (Figure S1c, Supporting Information). TEM analysis on the cycled particles further confirmed the lack of detectable defects and cracks within the shell. The SEM study of the Li-foil anodes before and after cycling showed formation of a smooth SEI layer on cycled Li foil without any Li or Li_2S (or Li_2S_2) precipitates or Li dendrites.

We have reported on the development of a hierarchical particle–shell architecture aimed to enhance long-term stability of the Li_2S-based cathodes. Such architecture provides multilevel protection against failure in the protective shelling material. Numerical modeling demonstrated an opportunity to significantly reduce stresses within the outer shell, which should further enhance mechanical stability of the particles and thereby enable effective operation of the electrochemical cells. As an example of the practical hierarchical composite, we synthesized C–Li_2S–C particles by using a simple solution-based method followed by carbon outer shell deposition through atmospheric pressure CVD. Electrochemical tests showed excellent capacity utilization and rate performance, enabled by embedding Li_2S (5–20 nm in size) into conductive material matrix. More importantly, by employing the hierarchical core–shell nanocomposite design, our Li_2S cathodes effectively mitigated polysulfide dissolution and achieved remarkable stability, significantly outperforming the best Li_2S cathodes reported in the recent literature. The hierarchical particle–shell architecture could be applied in many other high-energy volume-changing active materials (such as various metal fluorides and chlorides) that could be damaged or dissolved during undesirable interactions with electrolytes. Therefore, the hierarchical

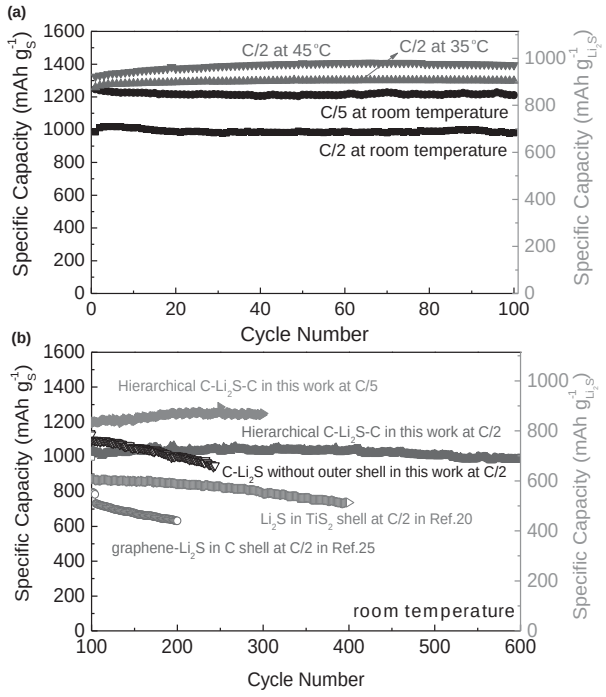

Figure 7. Electrochemical characterizations of the hierarchical C–Li_2S–C nanocomposite nanopowder samples: a) cycling performance at C/2 and C/5 rates at selected temperatures, b) capacity and cycle stability of the produced samples with and without shells in comparison with previous literature reports on shell-enclosed Li_2S powders.

particle–shell architecture and the chemical synthesis route demonstrated in this work may have a profound impact on drastic improvements of various energy storage chemistries and technologies.

Supporting Information

Supporting Information is available from the Wiley Online Library or from the author.

Acknowledgements

This work was partially supported by the Army Research Office (ARO grant W911NF-12-1-0259). Zhu was supported by the NSF grant DMR-1410936. The TEM used in this work was purchased using support from the NSF grant DMR-0922776.

Received: May 12, 2015
Revised: July 9, 2015
Published online: August 25, 2015

[1] D. Andre, S.-J. Kim, P. Lamp, S. F. Lux, F. Maglia, O. Paschos, B. Stiaszny, *J. Mater. Chem. A* **2015**, *3*, 6709.
[2] a) J. Zheng, J. Tian, D. Wu, M. Gu, W. Xu, C. Wang, F. Gao, M. H. Engelhard, J. G. Zhang, J. Liu, J. Xiao, *Nano Lett.* **2014**, *14*, 2345; b) X. Ji, K. T. Lee, L. F. Nazar, *Nat. Mater.* **2009**, *8*, 500; c) S. Zheng, Y. Chen, Y. Xu, F. Yi, Y. Zhu, Y. Liu, J. Yang, C. Wang, *ACS Nano* **2013**, *7*, 10995; d) H. D. Yoo, E. Markevich, G. Salitra, D. Sharon, D. Aurbach, *Mater. Today* **2014**, *17*, 110; e) Y. S. Su, Y. Fu, T. Cochell, A. Manthiram, *Nat. Commun.* **2013**, *4*, 2985; f) G. Salitra, E. Markevich, A. Rosenman, Y. Talyosef, D. Aurbach, A. Garsuch, *ChemElectroChem* **2014**, *1*, 1492; g) Y. S. Su, A. Manthiram, *Nat. Commun.* **2012**, *3*, 1166; h) P. G. Bruce, S. A. Freunberger, L. J. Hardwick, J. M. Tarascon, *Nat. Mater.* **2012**, *11*, 19; i) S. Lu, Y. Cheng, X. Wu, J. Liu, *Nano Lett.* **2013**, *13*, 2485; j) H. Yamin, E. Peled, *J. Power Sources* **1983**, *9*, 281.
[3] X. Ji, S. Evers, R. Black, L. F. Nazar, *Nat. Commun.* **2011**, *2*, 325.
[4] F. Wu, H. Kim, A. Magasinski, J. T. Lee, H.-T. Lin, G. Yushin, *Adv. Energy Mater.* **2014**, *4*, 1400196.
[5] X. Ji, L. F. Nazar, *J. Mater. Chem.* **2010**, *20*, 9821.
[6] a) X. He, J. Ren, L. Wang, W. Pu, C. Jiang, C. Wan, *J. Power Sources* **2009**, *190*, 154; b) M. Ebner, F. Marone, M. Stampanoni, V. Wood, *Science* **2013**, *342*, 716.
[7] W. Li, G. Zheng, Y. Yang, Z. W. Seh, N. Liu, Y. Cui, *Proc. Natl. Acad. Sci. USA* **2013**, *110*, 7148.
[8] H. Kim, J. T. Lee, G. Yushin, *J. Power Sources* **2013**, *226*, 256.
[9] Z. W. Seh, W. Li, J. J. Cha, G. Zheng, Y. Yang, M. T. McDowell, P. C. Hsu, Y. Cui, *Nat. Commun.* **2013**, *4*, 1331.
[10] a) S. Xiong, K. Xie, Y. Diao, X. Hong, *Electrochimica Acta* **2012**, *83*, 78; b) Z. Lin, Z. Liu, W. Fu, N. J. Dudney, C. Liang, *Adv. Funct. Mater.* **2013**, *23*, 1064.
[11] a) L. Suo, Y. S. Hu, H. Li, M. Armand, L. Chen, *Nat. Commun.* **2013**, *4*, 1481; b) F. Wu, J. T. Lee, N. Nitta, H. Kim, O. Borodin, G. Yushin, *Adv. Mater.* **2015**, *27*, 101.
[12] J. T. Lee, Y. Zhao, S. Thieme, H. Kim, M. Oschatz, L. Borchardt, A. Magasinski, W. I. Cho, S. Kaskel, G. Yushin, *Adv. Mater.* **2013**, *25*, 4573.
[13] S. Meini, R. Elazari, A. Rosenman, A. Garsuch, D. Aurbach, *J. Phys. Chem. Lett.* **2014**, *5*, 915.
[14] X. Liang, C. Hart, Q. Pang, A. Garsuch, T. Weiss, L. F. Nazar, *Nat. Commun.* **2015**, *6*, 5682.
[15] a) S.-H. Chung, A. Manthiram, *J. Phys. Chem. Lett.* **2014**, *5*, 1978; b) S. H. Chung, A. Manthiram, *Adv. Mater.* **2014**, *26*, 7352; c) W. Li, J. Hicks-Garner, J. Wang, J. Liu, A. F. Gross, E. Sherman, J. Graetz, J. J. Vajo, P. Liu, *Chem. Mater.* **2014**, *26*, 3403; d) Z. Zhang, Y. Lai, Z. Zhang, K. Zhang, J. Li, *Electrochim. Acta* **2014**, *129*, 55.
[16] N. Jayaprakash, J. Shen, S. S. Moganty, A. Corona, L. A. Archer, *Angew. Chem.* **2011**, *50*, 5904.
[17] a) R. Chen, T. Zhao, J. Lu, F. Wu, L. Li, J. Chen, G. Tan, Y. Ye, K. Amine, *Nano Lett.* **2013**, *13*, 4642; b) D. Wang, Y. Yu, W. Zhou, H. Chen, F. J. DiSalvo, D. A. Muller, H. D. Abruna, *Phys. Chem. Chem. Phys.* **2013**, *15*, 9051; c) D. S. Jung, T. H. Hwang, J. H. Lee, H. Y. Koo, R. A. Shakoor, R. Kahraman, Y. N. Jo, M. S. Park, J. W. Choi, *Nano Lett.* **2014**, *14*, 4418; d) Z. Li, Y. Jiang, L. Yuan, Z. Yi, C. Wu, Y. Liu, P. Strasser, Y. Huang, *ACS Nano* **2014**, *8*, 9295; e) J. J. Chen, Q. Zhang, Y. N. Shi, L. L. Qin, Y. Cao, M. S. Zheng, Q. F. Dong, *Phys. Chem. Chem. Phys.* **2012**, *14*, 5376; f) L. Zhu, H.-J. Peng, J. Liang, J.-Q. Huang, C.-M. Chen, X. Guo, W. Zhu, P. Li, Q. Zhang, *Nano Energy* **2015**, *11*, 746; g) J. Song, M. L. Gordin, T. Xu, S. Chen, Z. Yu, H. Sohn, J. Lu, Y. Ren, Y. Duan, D. Wang, *Angew. Chem.* **2015**, *54*, 4325.
[18] a) F. Wu, J. T. Lee, A. Magasinski, H. Kim, G. Yushin, *Part. Part. Syst. Characterization* **2014**, *31*, 639; b) F. Wu, A. Magasinski, G. Yushin, *J. Mater. Chem. A* **2014**, *2*, 6064.
[19] C. Nan, Z. Lin, H. Liao, M. K. Song, Y. Li, E. J. Cairns, *J. Am. Chem. Soc.* **2014**, *136*, 4659.
[20] Z. W. Seh, J. H. Yu, W. Li, P. C. Hsu, H. Wang, Y. Sun, H. Yao, Q. Zhang, Y. Cui, *Nat. Commun.* **2014**, *5*, 5017.
[21] L. Suo, Y. Zhu, F. Han, T. Gao, C. Luo, X. Fan, Y.-S. Hu, C. Wang, *Nano Energy* **2015**, *13*, 467.
[22] W. Zhou, Y. Yu, H. Chen, F. J. DiSalvo, H. D. Abruna, *J. Am. Chem. Soc.* **2013**, *135*, 16736.

[23] S. Jeong, D. Bresser, D. Buchholz, M. Winter, S. Passerini, *J. Power Sources* **2013**, *235*, 220.
[24] a) Z. W. Seh, H. Wang, P.-C. Hsu, Q. Zhang, W. Li, G. Zheng, H. b. Yao, Y. Cui, *Energy Environ. Sci.* **2013**, *7*, 672; b) L. Chen, Y. Liu, M. Ashuri, C. Liu, L. L. Shaw, *J. of Mater. Chem. A* **2014**, *2*, 18026; c) G. Ma, Z. Wen, J. Jin, Y. Lu, K. Rui, X. Wu, M. Wu, J. Zhang, *J. Power Sources* **2014**, *254*, 353; d) G.-C. Li, G.-R. Li, S.-H. Ye, X.-P. Gao, *Adv. Energy Mater.* **2012**, *2*, 1238.
[25] Z. Lin, C. Nan, Y. Ye, J. Guo, J. Zhu, E. J. Cairns, *Nano Energy* **2014**, *9*, 408.
[26] a) H.-J. Peng, J.-Q. Huang, M.-Q. Zhao, Q. Zhang, X.-B. Cheng, X.-Y. Liu, W.-Z. Qian, F. Wei, *Adv. Funct. Mater.* **2014**, *24*, 2772; b) X. Yang, L. Zhang, F. Zhang, Y. Huang, Y. Chen, *ACS Nano* **2014**, *8*, 5208; c) M. Q. Zhao, Q. Zhang, J. Q. Huang, G. L. Tian, J. Q. Nie, H. J. Peng, F. Wei, *Nat. Commun.* **2014**, *5*, 3410.
[27] M. Barghamadi, A. Kapoor, C. Wen, *J. Electrochem. Soc.* **2013**, *160*, A1256.
[28] L. Xiao, Y. Cao, J. Xiao, B. Schwenzer, M. H. Engelhard, L. V. Saraf, Z. Nie, G. J. Exarhos, J. Liu, *Adv. Mater.* **2012**, *24*, 1176.
[29] a) Y. Fu, C. Zu, A. Manthiram, *J. Am. Chem. Soc.* **2013**, *135*, 18044; b) K. Han, J. Shen, C. M. Hayner, H. Ye, M. C. Kung, H. H. Kung, *J. Power Sources* **2014**, *251*, 331; c) Y. Yang, G. Zheng, S. Misra, J. Nelson, M. F. Toney, Y. Cui, *J. Am. Chem. Soc.* **2012**, *134*, 15387; d) K. P. Cai, M. K. Song, E. J. Cairns, Y. G. Zhang, *Nano Lett.* **2012**, *12*, 6474; e) J. Guo, Z. Yang, Y. Yu, H. D. Abruna, L. A. Archer, *J. Am. Chem. Soc.* **2013**, *135*, 763.